Sensorless Vector Control of Induction Motor With On Line Parameters Adaptation

Gilberto Costa Drumond Sousa and Samuel Alves de Souza

Department of Electrical Engineering
Federal University of Espírito Santo - UFES
P.O. Box 01-9011 - 29060-970 - Vitória - Espírito Santo - Brazil
e-mail: g.sousa@ele.ufes.br

Abstract - This paper discusses the application of the synchronous frame Luenberguer observer technique to the problem of estimating simultaneously the speed and parameters of an induction motor (IM) operating under indirect vector control. A complete description of the technique, along with an insightful explanation of the rotor time constant adaptation mechanism are provided, in addition to simulation and experimental results.

I. INTRODUCTION

The advantages of using AC drives instead of DC drives are mentioned extensively in the literature. In particular, the robustness, low cost, and little maintenance of squirrel cage induction motor are frequently mentioned. When operating under vector control, high performance is added to the list.

There are two basic methods to implement a vector control, namely the direct and the indirect methods of field orientation [1]. In the direct method, the instantaneous position of the flux vector is required. Although this can be obtained through sensors, estimators are the most common, due to practical aspects. In fact, the use of flux sensors has the advantage of parameter insensibility, but this results in a reduction in robustness, and increases the cost. The estimators or observers obtain the flux position from the stator voltage and current measurements, based on the machine dynamic model. However, regarding costs, only voltage sensors represent added costs, since the current sensors are always present due to the need of a current loop in high performance drives. As the dynamic model of the machine is utilized, the control becomes sensitive to parameter variations. In the indirect method, the knowledge of the rotor time constant ($\tau_r = L_r / R_r$) is needed for achieving proper decoupling between flux and torque. The rotor inductance (L_r) varies with the saturation level, whereas the rotor resistance (R_r) is affected by temperature. In reality, both methods require the knowledge of the correct machine parameters to achieve proper decoupling between the flux and torque, i.e., perfect vector control.

The motor parameters are traditionally obtained through laboratory testes. Because the parameters varies with operating conditions, as described above, a lot of work has been done to obtain them on line. Some techniques depart from known parameters and track their variations. Others utilize methods such as extended Kalmam filter and recursive least squares, to determine the parameters. Self commissioning techniques have been proposed to obtain the relevant parameters during start-up, utilizing the knowledge of only the nameplate data, computing the parameters through test procedures done with standard voltage source inverters [2].

Sensorless vector control has been a topic of interest for drive systems researchers in recent years. Virtually all speed estimation techniques with practical application also require the knowledge of the motor parameters to correctly estimate the speed [3] [4]. This paper discusses the application of the Luenberger observer to the problem of simultaneously estimating the speed and parameters of an induction motor operation under indirect vector control. A detailed description of the technique is given, along with some insightful explanation of their adaptation mechanism.

II. SPEED ESTIMATION WITH ON-LINE PARAMETER ADAPTATION

Fig. 1 shows the basic structure of a Luenberger adaptive observer, that combined with an adaptive scheme, produces simultaneous estimation of speed ($\hat{\omega}_r$) and parameters ($\hat{R}_s$, $1/\hat{\tau}_r$) from stator voltages and currents measurements. It has been demonstrated in the literature [5] that, in order to simultaneously estimate the speed and rotor time constant ($\hat{\tau}_r$), it is required an extra excitation in the magnetizing current reference ($i^*_{ds\ superimposed}$), added to the fundamental frequency d^e-axis reference (i^*_{ds}). The block diagram of the indirect vector control system with speed estimation and on line parameters adaptation is shown in fig. 2.

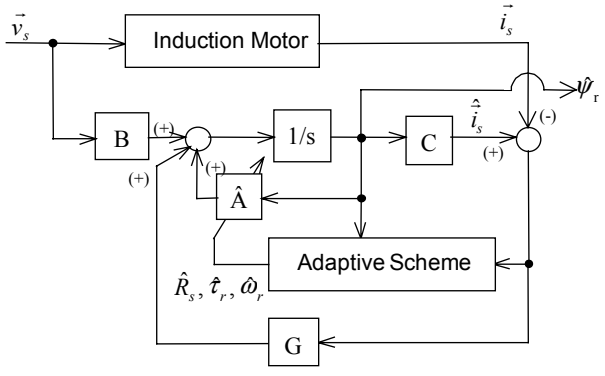

Fig. 1. Block diagram of a Luenberger adaptive observer.

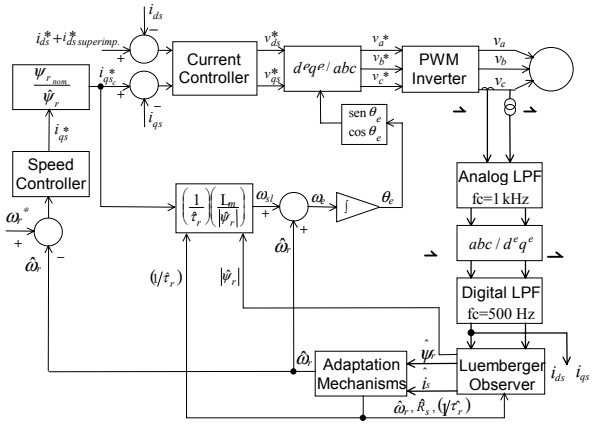

Fig. 2. Block diagram of the proposed system.

A. Mathematical Model

The synchronous frame state equations for the Luenberger observer are described below, and are based on the IM state equations. The "^" indicates an estimate of the actual variable or parameter. The state vector is composed of stator current and rotor flux vectors, $\hat{\vec{x}} = \left[\vec{i}_s \quad \vec{\psi}_r\right]^T$.

$$\frac{\mathrm{d}}{\mathrm{dt}}\hat{\vec{\mathrm{x}}} = \hat{\mathbf{A}}\hat{\vec{\mathrm{x}}} + \mathbf{B}\vec{\mathrm{v}}_\mathrm{s} + \mathbf{G}\left(\hat{\vec{\mathrm{i}}}_\mathrm{s} - \vec{\mathrm{i}}_\mathrm{s}\right) \tag{1}$$

$$\vec{\mathrm{i}}_\mathrm{s} = \mathbf{C}\vec{\mathrm{x}} \tag{2}$$

$\vec{v}_s$ is the stator voltage vector (input vector), $\mathbf{A}$ is the IM parameter matrix, $\mathbf{B}$ is the input and $\mathbf{C}$ the output matrices, respectively. By its turn, **A** can be written as:

$$\mathbf{A} = \begin{bmatrix} \mathbf{A_{11}} & \mathbf{A_{12}} \\ \mathbf{A_{21}} & \mathbf{A_{22}} \end{bmatrix}_\mathrm{s}$$

Where:

$$\mathbf{A_{11}} = -\left\{\frac{\mathrm{R_s}}{\sigma \mathrm{L_s}} + \frac{1-\sigma}{\sigma\tau_\mathrm{r}}\right\}\mathbf{I} + \omega_\mathrm{e}\mathbf{J} = \mathrm{a_{r11}}\mathbf{I} + \mathrm{a_{i11}}\mathbf{J}$$

$$\mathbf{A_{12}} = \frac{\mathrm{L_m}}{\sigma \mathrm{L_s L_r}}\left\{\frac{1}{\tau_\mathrm{r}}\mathbf{I} - \omega_\mathrm{r}\mathbf{J}\right\} = \mathrm{a_{r12}}\mathbf{I} + \mathrm{a_{i12}}\mathbf{J}$$

$$\mathbf{A_{21}} = \frac{\mathrm{L_m}}{\tau_\mathrm{r}}\mathbf{I} = \mathrm{a_{r21}}\mathbf{I}$$

$$\mathbf{A_{22}} = -\frac{1}{\tau_\mathrm{r}}\mathbf{I} - (\omega_\mathrm{e} - \omega_\mathrm{r})\mathbf{J} = \mathrm{a_{r22}}\mathbf{I} + \mathrm{a_{i22}}\mathbf{J}$$

$$\mathbf{B_1} = \frac{1}{\sigma \mathrm{L_s}}\mathbf{I} = \mathrm{b_1}\mathbf{I}$$

$$\mathbf{C} = \begin{bmatrix}\mathbf{I} & 0\end{bmatrix} \quad \mathbf{I} = \begin{bmatrix}1 & 0 \\ 0 & 1\end{bmatrix} \quad \mathbf{J} = \begin{bmatrix}0 & -1 \\ 1 & 0\end{bmatrix} \quad \mathbf{K} = \begin{bmatrix}0 & 1 \\ 1 & 0\end{bmatrix}$$

In $\hat{\mathbf{A}}$ the ω_r, R_s e τ_r are replaced by the estimated values $\hat{\omega}_r$, $\hat{R}_s$ e $\hat{\tau}_r$, that are updated as discussed later.

The observer gain matrix $\mathbf{G}$ is designed such that the observer poles are proportional to the IM poles, that is inherently stable [5].

$$\mathbf{G} = \begin{bmatrix} \mathrm{g_1} & \mathrm{g_2} & \mathrm{g_3} & \mathrm{g_4} \\ -\mathrm{g_2} & \mathrm{g_1} & -\mathrm{g_4} & \mathrm{g_3} \end{bmatrix}^\mathrm{T} \tag{3}$$

Where:

$$\mathrm{g_1} = (\mathrm{k}-1)(\mathrm{a_{r11}} + \mathrm{a_{r22}})$$

$$\mathrm{g_2} = (\mathrm{k}-1)\mathrm{a_{i22}}$$

$$\mathrm{g_3} = (\mathrm{k}^2 - 1)(\mathrm{ca_{r11}} + \mathrm{a_{r21}}) - \mathrm{c}(\mathrm{k}-1)(\mathrm{a_{r11}} + \mathrm{a_{r22}})$$

$$\mathrm{g_4} = -\mathrm{c}(\mathrm{k}-1)\mathrm{a_{i22}}$$

$$\mathrm{c} = \frac{\sigma \mathrm{L_s L_r}}{\mathrm{L_m}} \text{ and } k \geq 1 \text{ (proportionality constant)}$$

R_s, R_r are the stator and rotor resistance, L_s, L_r stator and rotor inductance, L_m is the mutual inductance, σ is the leakage coefficient ($\sigma = 1 - L^2{}_m / L_s L_r$), τ_r is the rotor time constant ($\tau_r = L_r / R_r$), ω_r is the motor speed in electric rad/s, whereas ω_e is the stator angular frequency.

B. Adaptation Mechanism

The Luenberger observer can be viewed as an "MRAS", where the IM is considered the reference model, and the observer the adjustable model. Of course, these schemes must ensure that, when the estimates $\hat{\omega}_r$, $\hat{R}_s$ and $\hat{\tau}_r$ converge to the actual values ω_r, R_s, τ_r, the state estimate $\hat{\vec{x}}$ will become identical to the actual state vector $\vec{x}$, i.e., zero estimate error is achieved.

The error between the states $\vec{x}$ and $\hat{\vec{x}}$ is utilized to drive the adaptive schemes for rotor speed $(\hat{\omega}_r)$, stator resistance $(\hat{R}_s)$, and rotor time constant $\hat{\tau}_r$. These adaptation schemes are based on the Lyapunov stability criteria, and just listed below for the sake of completeness [5].

$$\frac{\mathrm{d}}{\mathrm{dt}}\hat{\mathrm{R}}_\mathrm{s} = -\lambda_1\left(\mathrm{ei_{ds}}\hat{\mathrm{i}}_\mathrm{ds} - \mathrm{ei_{qs}}\hat{\mathrm{i}}_\mathrm{qs}\right) \tag{4}$$

$$\frac{\mathrm{d}}{\mathrm{dt}}\left(\frac{1}{\hat{\tau}_\mathrm{r}}\right) = \frac{\lambda_2}{\mathrm{L_r}}\left\{\mathrm{ei_{ds}}\left(\hat{\psi}_\mathrm{dr} - \mathrm{L_m}\hat{\mathrm{i}}_\mathrm{ds}\right) + \mathrm{ei_{qs}}\left(\hat{\psi}_\mathrm{qr} - \mathrm{L_m}\hat{\mathrm{i}}_\mathrm{qs}\right)\right\} \tag{5}$$

$$\frac{\mathrm{d}}{\mathrm{dt}}\hat{\omega}_\mathrm{r} = \frac{\lambda}{\mathrm{c}}\left(\mathrm{ei_{ds}}\hat{\psi}_\mathrm{qr} - \mathrm{ei_{qs}}\hat{\psi}_\mathrm{dr}\right) \tag{6}$$

Where $ei_{ds} = i_{ds} - \hat{i}_{ds}$ and $ei_{qs} = i_{qs} - \hat{i}_{qs}$.

C. Phasor Analysis of the adaptation mechanism

An insight on the operation of the rotor time constant adaptation mechanism will be provided here. The adaptive system consists of an integral controller (5) that acts upon an error signal (U) obtained as the inner product of the d-q axis stator current error vector ($\vec{e}i_s$) and the flux vector ($\hat{\vec{\varphi}}_r - L_m \hat{\vec{i}}_s$) as indicate by (7).

$$U = ei_{ds}\left(\hat{\psi}_{dr} - L_m \hat{i}_{ds}\right) + ei_{qs}\left(\hat{\psi}_{qr} - L_m \hat{i}_{qs}\right) \qquad (7)$$

In fact, by using the steady state inverse gamma model (Γ^{-1}) for the induction machine [6] shown in Fig 3, along with phasor diagram of Fig. 4, the behavior of the error signal can be illustrated. Fig. 3 shows a circuit that clearly indicates the partition of the stator current $\vec{i}_s$ into two components: $\vec{i}_{s\varphi}$ which controls the level of the rotor flux, and $\vec{i}_{sT}$ which controls the air gap power and hence the torque.

The slip relation associated with field orientation is simply an expression of the required equality of voltages produced by $\vec{i}_{s\varphi}$ in the magnetizing branch and $\vec{i}_{sT}$ in the rotor branch, in steady state:

$$\vec{i}_{s\varphi}\left(j\frac{L_m}{L_r}X_m\right) = \vec{i}_{sT}\left(\frac{L^2 m R_r}{L^2 r s}\right)$$

This result clearly demonstrates that $\vec{i}_{s\varphi}$ and $\vec{i}_{sT}$ are orthogonal components, and that the slip frequency is related to the magnitudes of the current components by the relation:

$$\omega_{sl} = s\omega_e = \frac{1}{\tau_r}\frac{\vec{i}_{sT}}{\vec{i}_{s\varphi}} = \frac{L_m}{\vec{\psi}_r}\frac{1}{\tau_r}\vec{i}_{sT} \qquad (8)$$

where

$$\vec{\psi}_r = L_m \vec{i}_{s\varphi} \quad \tau_r = \frac{L_r}{R_r}.$$

In indirect vector control, the slip relation of (8) is employed directly to obtain the correct partition of the stator current into the torque ($\vec{i}_{sT}$) and field components ($\vec{i}_{s\varphi}$). This concept can be expressed by using current division to relate $\vec{i}_s$ and $\vec{i}_{sT}$ in Fig. 3:

$$\vec{i}_{sT} = -\frac{L_r}{L_m}\vec{i}_r = \vec{i}_s \frac{j\left(\frac{L_m}{L_r}\right)X_m}{\left(\frac{L_m}{L_r}\right)^2\left(\frac{R_r}{s}\right) + j\left(\frac{L_m}{L_r}\right)X_m}$$

where the value of s is calculated from (8). Rearranging and simplifying yields:

$$\vec{i}_r = \frac{-j\omega^*_{sl} L_m \vec{i}_s}{Rr + j\omega^*_{sl} L_r} \qquad (9)$$

where ω^*_{sl} is the slip frequency from (8). In effect, with the correct value of ω^*_{sl}, (9) yields the proper rotor current $\vec{i}_r$ to counterbalance the torque component $\vec{i}_{sT}$, and the correct partition of the stator current is assured.

In the steady state the axis quantities are all constants, and it is easily shown that the stator d and q current components have the same magnitude as the phasor current components $\vec{i}_{s\varphi}$ and $\vec{i}_{sT}$. It also easily shown that, there is a complete equivalence between the d-q equations and the equivalent circuit of Fig. 3 at steady state conditions.

Utilizing the speed control system of Fig. 2, let us consider a particular condition, where the system utilizes the actual speed in the control loop, the correct stator resistance value, and only the rotor time constant adaptation mechanism is implemented. The flux current command (i^*_{ds}) is assumed constant, whereas the torque current command (i^*_{qs}) varies to yield the necessary torque required by the load, such as to maintain the speed at the reference value (ω^*_r). By utilizing (9), phasor diagrams will be developed for the situations: (a) $\hat{\tau}_r = \tau_{r(actual)}$ and (b) $\hat{\tau}_r > \tau_{r(actual)}$.

The reference current $\vec{i}_s{}^*$ ($i^*_{qs} - j\,i^*_{ds}$) establishes the position of the flux phasor $L_m\vec{i}_s$. The rotor induced voltage $\left(-j\omega^*_{sl}L_m\vec{i}_s\right)$ lags $\vec{i}_s$ by an angle of 90°. The phase angle of the rotor self impedance ($\varphi_r = tg^{-1}(\omega^*_{sl}\hat{\tau}_r)$) then defines the position of the rotor current ($\vec{i}_r$).

If $\hat{\tau}_r = \tau_{r(actual)}$, the rotor current will be exactly in opposition to the torque command current i^*_{qs} (i_{sT}) and correct field orientation is achieve. The rotor flux ($\vec{\psi}_r$) which is orthogonal to $\vec{i}_r$, will be aligned with i_{ds} ($i_{s\varphi}$) in the d-axis as illustrated in fig. 4(a). The flux linkage vector $L_r\vec{i}_r$ has the effect of canceling the quadrature component of $L_m\vec{i}_s$.

If $\hat{\tau}_r > \tau_{r(actual)}$, a smaller value of ω^*_{sl} is obtained. The rotor induced voltage decreases, the rotor self impedance decreases, the torque command current increases, the stator current increases, and the rotor flux increases. Thus the rotor current will no longer lie in the q axis but is pushed down towards the d axis. The rotor flux will move away from d axis, counterclockwise, so as to maintain orthogonality with $\vec{i}_r$, as shown in fig. 4(b).

If the estimated rotor time constant is greater then the actual value as shown in fig. 4(b), the estimated slip frequency becomes smaller than the correct value, causing an increase in the q-axis stator current component, such that current error vector ($\vec{e}i_{s1}$) lags the flux vector ($\hat{\vec{\varphi}}_{r1} - L_m\hat{\vec{i}}_{s1}$) by an angle smaller than 90°, resulting in a positive error U of (7). As a consequence, the integral controller of (1) increases $1/\hat{\tau}_r$ (resulting in a decrease in $\hat{\tau}_r$), until the error is driven to zero. Opposite behavior occurs when the estimated rotor time constant is smaller than the actual value but this is not discussed here.

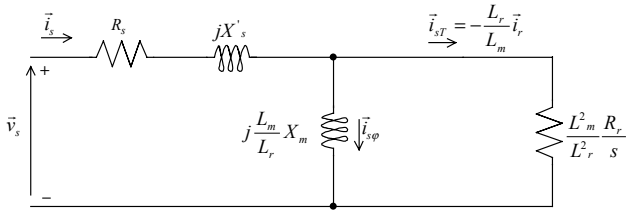

Fig. 3. Inverse gamma (Γ^{-1}) equivalent circuit for induction motor.

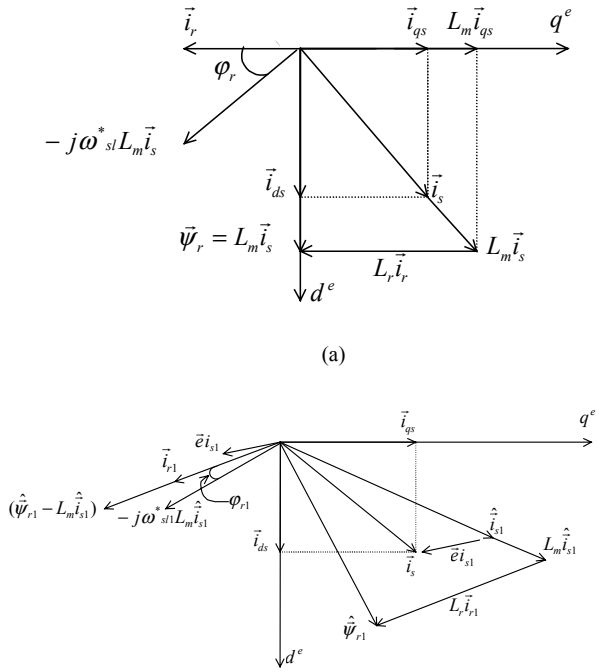

Fig. 4. Phasor diagram of adaptation mechanism.
(a) $\hat{\tau}_r = \tau_{r(actual)}$, (b) $\hat{\tau}_r > \tau_{r(actual)}$.

III. SIMULATION STUDIES

The proposed system (Fig. 2) was simulated using SIMNON language [7]. Simulation studies were initially conducted to validate the proposed system, as well as to determine the proper gains for the adaptation mechanisms.

The Luenberger adaptive observer and the current control loop were implemented in a synchronously rotating reference frame such that a relatively large integration step could be used (200 μs), with minimum numerical errors. Low-Pass filters were utilized to condition the current and voltage signals needed for the observer.

The system behavior was initially investigated for a low speed (0.10 pu) and partial load torque (0.35 pu) condition, as illustrated in Fig. 5. The stator resistance and the inverse of the rotor time constant were intentionally set to an incorrect initial value, 1.5 times the nominal ones, and the system was brought to a steady state conditions before t=0 sec. The stator resistance, the rotor time constant estimation, and the superimposing of AC components on the field current started at t=2 sec. Then simultaneous estimation causes the motor speed and estimated parameters to converge to the correct values in a few seconds. Other speed and torque conditions were also investigated, but are not discussed here.

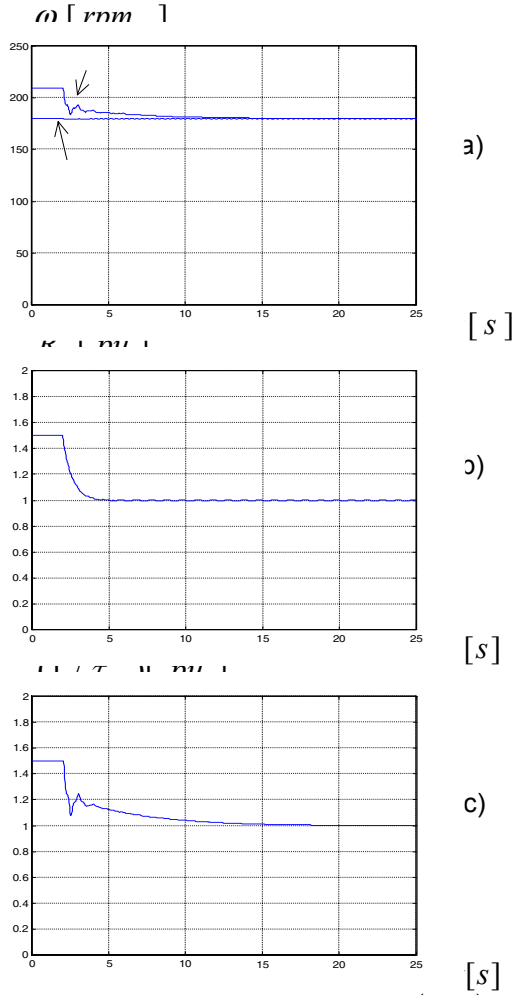

Fig. 5 Simultaneous estimation of ω_r, R_s, and $(1/\tau_r)$ at ω^*_r = 180 rpm, T_L = 0.35 pu.

IV. EXPERIMENTAL STUDIES

After the simulation study, a prototype system was implemented, as shown in Fig. 6. It utilizes a Host PC with an embedded Texas Instrument's TMS320C25 DSP based control board from Dalanco Spry [8][9]. Except for the A/D and D/A converter, all control functions are implemented with a 200 µs sampling time. The man-machine interface is implemented in the Host PC, that is responsible for starting / stopping the system, establishing the speed reference, as well as capturing the system internal variables and graphically displaying them. Experimental results of the parameter estimation is shown in Fig. 7 for a 5 hp, 4 poles induction motor drive, for an identical condition illustrated in Fig. 6 (speed = 0.10 pu, and load torque = 0.35 pu). The speed estimate is utilized to close the speed loop, and he initial values of stator and inverse of rotor time constant in the observer are set to 1.5 times the nominal values. The estimation starts at t=4 sec., and it can be seen that, while stator resistance and rotor time constant converge to their correct values, the actual speed approaches the estimated speed. A small, essentially constant, steady state speed estimation error was observed at different speed and torque conditions. It can be attributable to several factors: non-linearities in the voltage and current sensing circuits, leakage inductance saturation, A/D resolution, etc.

Fig. 8 shows the estimates for rotor flux components. The effects of the low frequency AC component injection ($i^*_{ds\ superimposed}$) are clearly seen on the d-axis component, as well as its convergence to the correct value, as the parameter estimates converge to their correct value. The flux q-axis component converges to zero, as expected for correct vector control.

V. CONCLUSIONS

This paper discussed the application of the Luenberger observer to the problem of estimating simultaneously the motor speed and the motor parameters of an induction motor operation under indirect vector control. An insightful explanation of the rotor time constant adaptation mechanism was provided, along with simulation and experimental results. The studies verify the validity of the synchronous frame Luenberguer observer technique applied to an indirect vector control system.

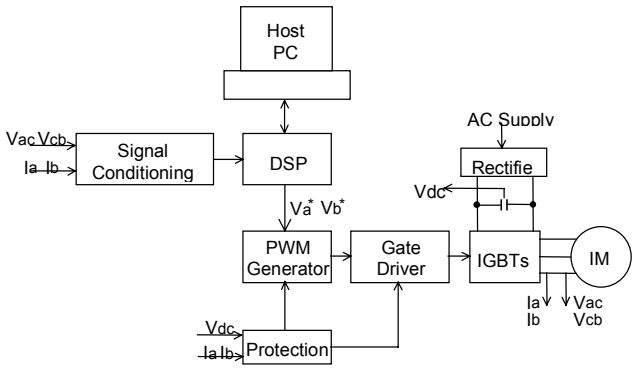

Fig. 6. Block diagram of experimental system.

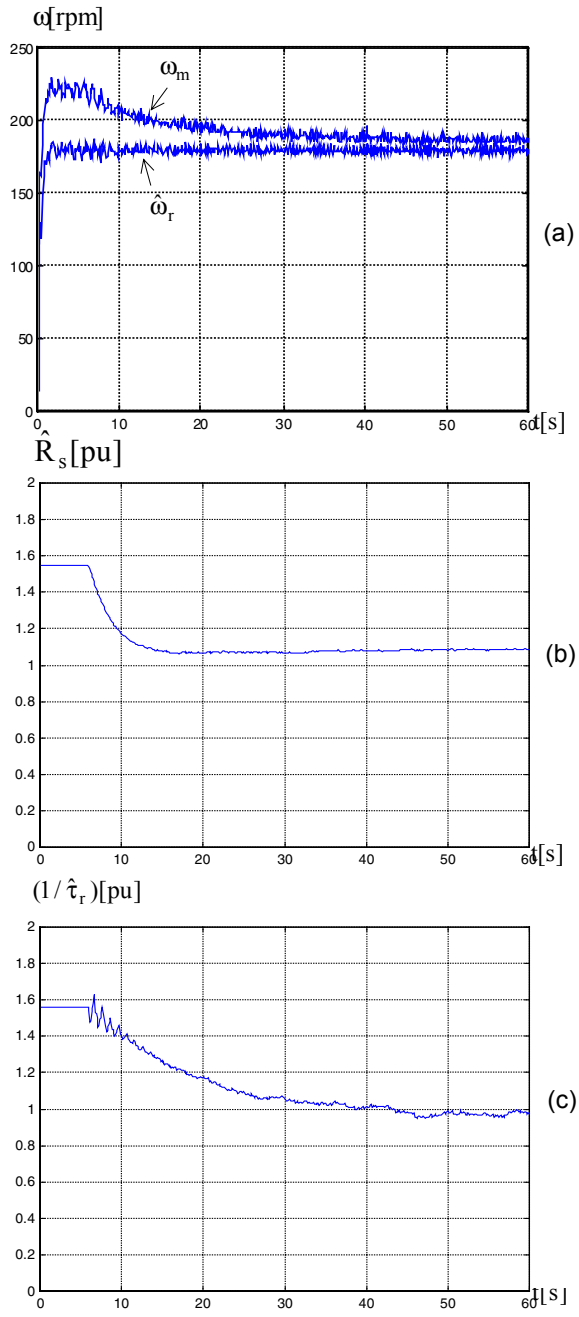

Fig. 7: Experimental result for ω_r^* = 0.10 pu and T_L= 0.35 pu.

VI. REFERENCES

[1] B. K. Bose, Power Eletronics and AC Drives, Prentice-Hall, New York, 1986.

[2] J. L. Silvino, B. C. Jr. Rabelo, "Autocomissioned Induction Machine Vector Control", COBEP'97, pp. 127-132, 1997.

[3] Eliane Patrício Machado Pedrini, *"Um Estudo Comparativo de Técnicas de Estimação da Velocidade do Motor de Indução Baseadas na Força Contra-Eletromotriz"*, Master's Dissertation, Federal University of Espírito Santo, Brazil, 1998.

[4] G. C. D. Sousa and A. P. S. S. Rabello, "Application of the Luenberger Observer to the Sensorless Speed Control of an Induction Motor Drive: Analysis and Implementation", 5th Brazilian Power Eletronics Conference - COBEP'99,pp 681-686, 1999.

[5] H. Kubota, K. Matsuse, "Speed Sensorless Field-Oriented Control of Induction Motor with Rotor Resistance Adaptation", IEEE Transactions on Industry Applications, Vol. 30, No. 5 September/October 1994.

[6] K. B. Nordin, D. W. Novotny, D. S. Zinger, “The Influence of Motor Parameter Deviations in Feedfoorward Field Orientation Drive Systens”, IEEE Transactions on Industry Applications, Vol. 21, No. 4 July/August 1985.
[7] Simnon User's Guide for MS-DOS Computers, Version 3.2, Janeiro 1993.
[8] TMS320CX User Guide, Texas Instruments Inc., 1990.
[9] Dalanco Spry Model 250, Data Acquisition and Signal processing Board Documentation, 1990

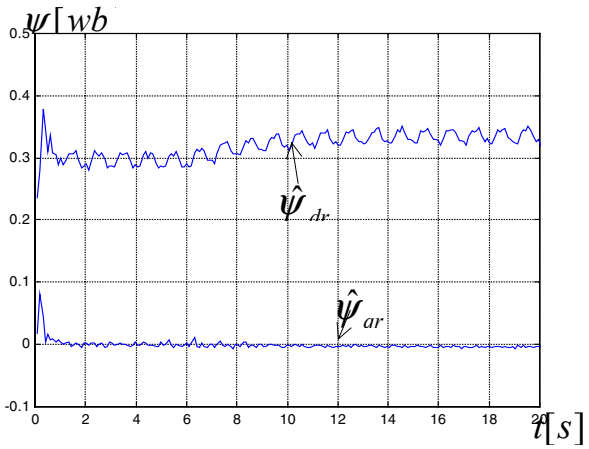

Fig. 8 – Rotor flux estimates ($\hat{\psi}_{dr}$) and ($\hat{\psi}_{qr}$) for the same condition of Fig. 7.